Identification of Faults and Potential Faults in Low Voltage Lines

Gonçalo Gil
Instituto Superior Técnico
Lisboa, Portugal
Email: goncalo.gil@outlook.com

***Abstract*—Power cables, responsible for electric energy transmission, are subject to ageing processes that continuously reduce the power cable capabilities to withstand the necessary efforts of its function, leading to eventual failure and an unpredictable power outage.**

In this research, it is intended to study a methodology capable of detecting these phenomenons based on electric variables to detect faults and potential faults in low voltage lines.

For this, the influence of thermal ageing and water trees in power cables insulators were studied, and simulations were developed based on the main changes discovered. The results of the various simulations were then compared through a process where most of the conductors' voltages are compressed into seven parameters.

This comparison showed that each of these phenomenons changed all seven parameters in different ways. In the case of the water trees, some of them were not detected. However, when discovered, it was possible to identify its location in the power cable.

Finally, it was made a flowchart that describes a process where the phenomenon suffered by the power cable is estimated based on the seven parameters, which in turn reflect the electric variables of its conductors.

I. Introduction

In the last years, with the rise of consumers and the development of micro-production with renewable energies, there was an increase of load and new profiles of consumption which provokes additional ageing of the power cables. As the detrition is stronger, the power outage becomes more frequent.

Beyond the increase of interruptions, there is a requirement for greater control of the network, which makes energy operators under huge pressure to reduce the downtime. So there is a need to reduce the duration of interruptions, and the solution can not be only the replacement of elements, it is necessary to identify faults and potential faults.

It is necessary a system that can identify faults and potential faults automatically and remotely without interfering in the power system, and it should also be able to be installed under working networks. A method like this would allow power operators to optimize the lifetime of power cables and plan the maintenance of infrastructures more efficiently, leading to a reduction of maintenance costs, reduction of component wasting and, a better power system.

The approach of this work is to study how some common phenomenons affect the power cables to then simulate these phenomenons and analyze the impact they have on electrical variables. The final goal is to identify patterns that allow doing the reversal process, estimate how and how much was the power cable affected by these phenomenons through an analysis of electrical variables.

II. Power Cable Deterioration

When talking about power cable ageing, the component more affected by these phenomenons is the insulator, which function is to avoid an electric current flux between the different conductors existing in the power cable. So, for having high dielectric strength, supporting high mechanical stresses, slow ageing, heat resistance, and reduced maintenance costs, Cross-linked polyethylene (XLPE) is the dielectric preferred for power cables. [1][2]

With the increase in the operation time, power cables' insulators lose their capacities until there's a permanent failure of the power cable. This degradation can occur in different ways, called ageing processes, that change the insulators' properties in different ways.

A. Thermal Ageing

A study has subjected XLPE samples to various temperatures during different periods and then has registered the evolution of properties of the samples [3]. One example is the evolution of relative permittivity of the insulator through the ageing time, where a replica is present in fig. 1.

The results show that for low temperatures, $80\,^{\circ}\mathrm{C}$ and $100\,^{\circ}\mathrm{C}$, the electric permittivity variation is not significant, although there's a slight increase in the mean value. However, for high temperatures, $100\,^{\circ}\mathrm{C}$ and $140\,^{\circ}\mathrm{C}$, there is a considerable increase of the electric permittivity after a specific ageing time. [3]

So, having in mind that a power cable operates at various temperatures during its life, its relative permittivity tends to increase with the operation time in real situations.

On the other hand, by analyzing the results in fig. 1 at zero ageing time, it is visible that the relative permittivity tends to decrease with a temperature increase.

Therefore, in an overall situation, an increase in the relative permittivity may reflect the thermal ageing of the cable. A decrease of permittivity may indicate an increment of the temperature.

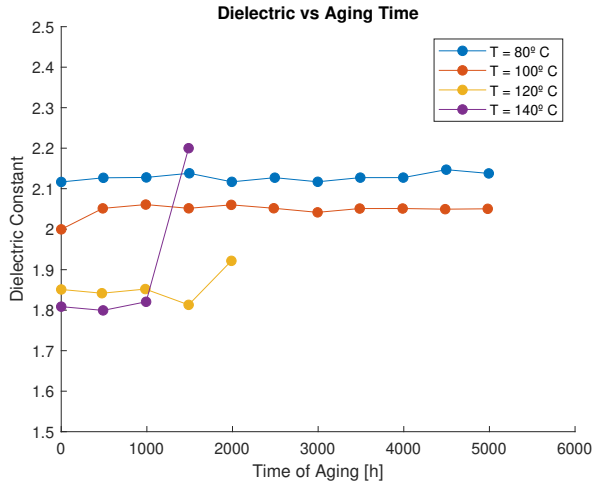

Fig. 1. Relative permittivity evolution for ageing time (Adapted from *Dielectric and Mechanical Behavior of Cross-Linked Polyethylene Under Thermal Aging* [3])

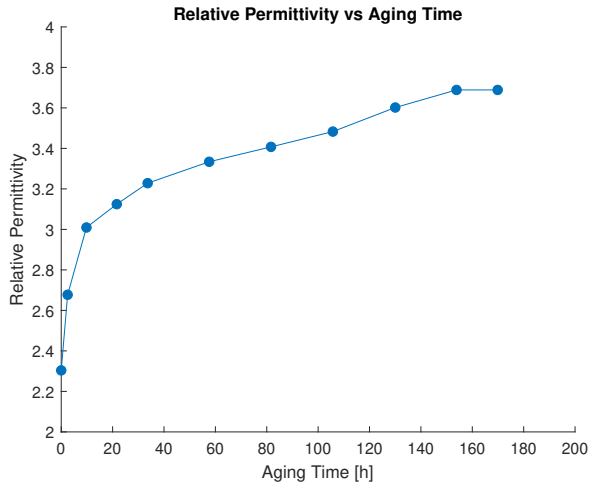

Fig. 2. Water Tree relative permittivity evolution for ageing time (Adapted from *The Effect of Water Treeing on the Electric Field Distribution of XLPE* [4])

B. Water Trees

Another study [4] has exposed XLPE samples to sandblast to create the defects propitious to the formation of *Water Tree* (WT). This exposure had the goal to develop a uniform WT layer after an ageing process. The ageing process used consisted of the application of a $5\,\mathrm{kV}$ voltage at $10\,\mathrm{kHz}$ to the sandblasted XLPE samples, while dipped in a $NaCl$ solution. This process was then run for different periods, and the evolution of the damaged XLPE samples concerning time duration was registered. [4]

It allowed the plot of the relative permittivity of the damaged zone concerning ageing process time duration, replicated in fig. 2. From fig. 2, it's visible, that a WT causes a relative permittivity increase in the damaged area that can reach values over $60\,\%$ higher than a new XLPE sample.

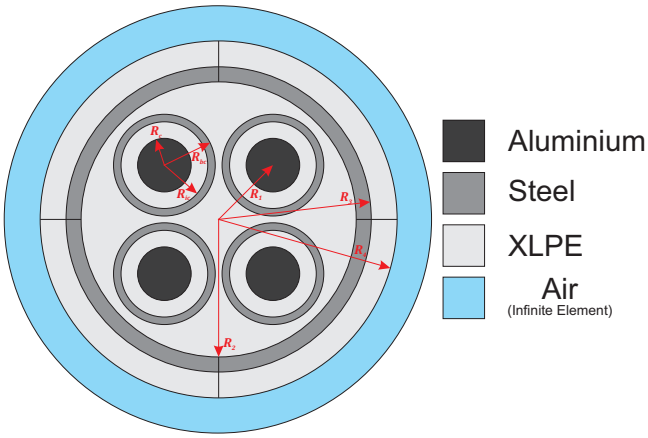

Fig. 3. Cross-section of the power cable model

TABLE I
POWER CABLE MODEL DIMENSIONS

Variable	**Length** [mm]
R_c	1.78
R_{ic}	2.88
R_{bc}	3.38
R_1	5.10
R_2	9.14
R_3	10.14
R_4	11.86

TABLE II
CABLE MATERIALS PROPERTIES

	ϵ_r	σ [S m^{-1}]
Aluminium	1	3.5×10^7
Steel	1	1×10^7
XLPE	2.3	1×10^{-18}

III. 3D Model Definition

A. Model's Structure

Before the simulation of these phenomenons, a model of a power cable was developed in a Finite Element Method Software (FEMS). For this, the cross-section presented in fig. 3 was sketched with the dimensions from table I and then extruded for $20\,\mathrm{mm}$, creating a set of domains for whom the materials were assigned accordingly with fig. 3 and table II.

B. Methodology

The process described before generated a set of nine conductors, that from now on will be identified as fig. 4 represents. From these nine conductors, four of them (C_1, C_2, C_3 and C_N) will have imposed voltages, and the five sheaths (S_1, S_2, S_3, S_N and S_E) will have an electric potential dependent on the first four conductors and XLPE electrical properties.

The imposed electric potential for the conductors C_1, C_2, C_3 and C_N, will be a pure sinusoidal three-phases and balanced system, as defined in eq. (1) and will be identical to all the simulations.

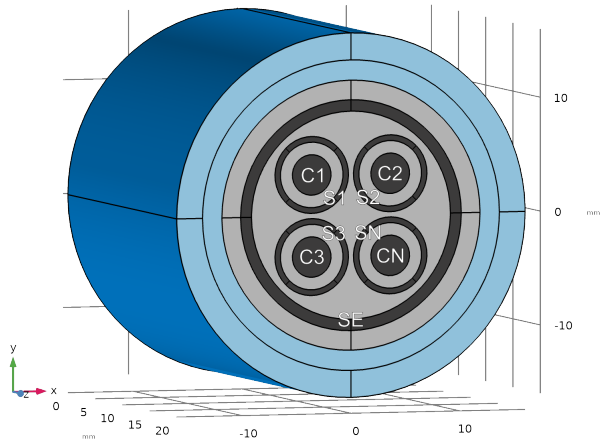

Fig. 4. Conductor's identification

$$\begin{cases} V_{C_1} = 230\sqrt{2}\cos\left(2\pi 50t\right) \\ V_{C_2} = 230\sqrt{2}\cos\left(2\pi 50t + \frac{2\pi}{3}\right) \\ V_{C_3} = 230\sqrt{2}\cos\left(2\pi 50t - \frac{2\pi}{3}\right) \\ V_{C_N} = 0 \end{cases} \quad [\text{V}] \tag{1}$$

It is relevant to state that, for this case, there is no harmonic or any noise in these electric potentials applied.

The imposed conditions in conductors C_1, C_2, C_3 and C_N will affect the sheaths' electric potential that will be calculated through time-dependent simulations, and if as expected, will change depending on XLPE changes. These simulations' outputs will be analyzed with a methodology which starts with the definition of the three electric potential differences defined in eq. (2).

$$\begin{cases} V_{\Delta 1} = V_{C_1} - V_{S_1} \\ V_{\Delta 2} = V_{C_2} - V_{S_2} \\ V_{\Delta 3} = V_{C_3} - V_{S_3} \end{cases} \tag{2}$$

These three electric potential differences were then plotted in a 3D graph where $V_{\Delta 1}$ were assigned to $\boldsymbol{X}$, $V_{\Delta 2}$ to $\boldsymbol{Y}$ and $V_{\Delta 3}$ to $\boldsymbol{Z}$, and it was verified that the plot of these voltages defined a pattern described by an ellipse inserted in an arbitrary 3D plane, as presented in fig. 5. So, the 3D representation in fig. 5 can be simplified by looking to the 3D ellipse from the normal perspective to its plane. For this, it is required to determine the plane's equation where the 3D ellipse is contained by adjusting equation expressed in (3) to the ellipse points, and then calculate the necessary transformations to align plane's normal with $\boldsymbol{Z}$ vector, as represented in fig. 6. These transformations needed can be summarized into two rotations (α and β), whose amplitudes are calculated through eq. (4).

$$Ax + By + Cz + D = 0 \tag{3}$$

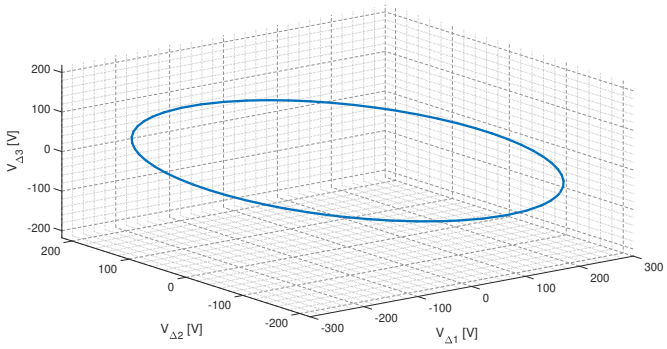

Fig. 5. 3D pattern of V_Δ set of voltages obtained during a normal operating condition of the three-phase underground cable

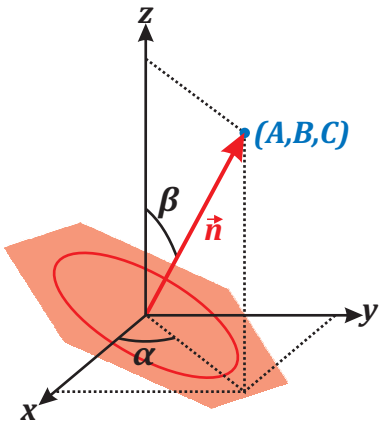

Fig. 6. Ellipse's plane orientation

$$\begin{cases} \alpha = \arctan\left(\frac{B}{A}\right) \\ \beta = \arctan\left(\frac{\sqrt{A^2+B^2}}{C}\right) \end{cases} \tag{4}$$

The output of these transformations is an ellipse in a two-dimensional graph, which can be analytically expressed as in eq. (5), or summarized into seven geometric parameters as depicted in fig. 7. These two methods of describing an ellipse are linked through eq. (6) to eq. (9) so, by fitting the eq. (5) to the new ellipse's points, the initial 3D pattern can be summarized into seven parameters: α, β, a, b, x_0, y_0 and θ.

$$Ex^2 + Fxy + Gy^2 + Hx + Iy + J = 0 \tag{5}$$

$$a, b = \frac{-\sqrt{2\left(EI^2 + GH^2 - FHI + (F^2 - 4EG)J\right)}}{F^2 - 4EG} \times \\ \times \sqrt{\left((E+G) \pm \sqrt{(E-G)^2 + F^2}\right)} \tag{6}$$

$$x_0 = \frac{2GH - FI}{F^2 - 4EG} \tag{7}$$

$$y_0 = \frac{2EI - FH}{F^2 - 4EG} \tag{8}$$

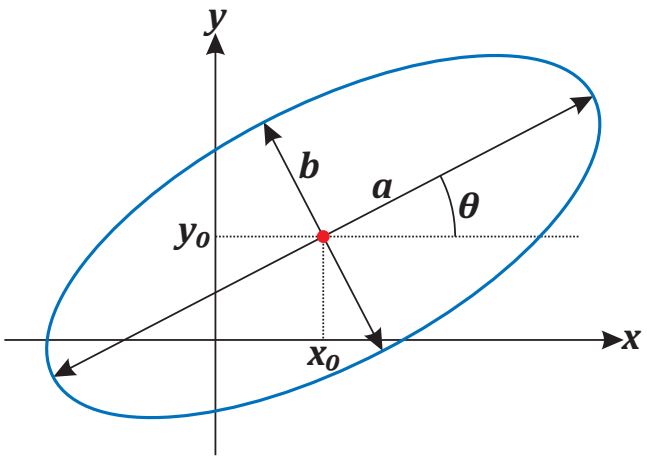

Fig. 7. 2D ellipse geometric parameters

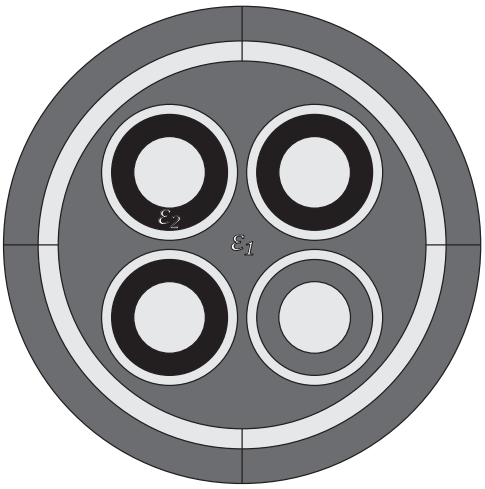

Fig. 8. XLPE's domain division

TABLE III
REFERENCE SIMULATION RESULTS

α [°]	β [°]	a [V]	b [V]	x_0 [V]	y_0 [V]	θ [°]
43.19	55.61	281.67	257.54	0.03	0.02	−58.98

$$\theta = \begin{cases} \arctan\left(\frac{(G-E-\sqrt{(E-G)^2+F^2})}{F}\right), & B \neq 0 \\ 0°, \ B = 0, \ E < G \\ 90°, \ B = 0, \ E > G \end{cases} \quad (9)$$

C. Reference Simulation

Having this methodology defined allows comparing different simulations through these seven parameters. To have a reference value for this set of variables, the model described in this section was simulated, leading to the results in table III.

IV. Thermal Ageing

A. Model Adjustments

Based on the XLPE behaviour due to thermal ageing, presented in section II-A, simulations in a FEMS were developed to analyze the outcome of insulator's thermal ageing.

Since the phase conductors are the main thermal source in a power cable [5], the XLPE's local average temperature will be higher as the closer it is from the phase conductors. So, having in mind the study [3], presented in section II-A, these regions will manifest changes earlier. So, this simulation study will divide the model's XLPE domain into two groups, as fig. 8 shows.

Group 1 is formed by the XLPE's regions furthest from the phase conductors where the relative electric permittivity (ϵ_1) is fixed to 2.1. Group 2 is composed of the domains nearest from these conductors and the relative electric permittivity of this group (ϵ_2) will be changed due thermal ageing.

Assuming the thermal ageing will be uniform through the cable length, to simplify the model and reduce calculation time, only two-dimensional simulations of the cross-section presented in fig. 3 were used.

TABLE IV
THERMAL AGEING DEVIATION RESULTS

$\epsilon_2 - \epsilon_1$	α[%]	β[%]	a[%]	b[%]	x_0[%]	y_0[%]	θ[%]
−0.3	0.12	−0.05	4.36	5.32	−16.74	8.52	0.08
−0.15	0.06	−0.02	2.13	2.59	3.23	6.55	0.03
0	0	0	0	0	0	0	0
0.2	−0.07	0.02	−2.71	−3.26	−25.14	−5.81	−0.03
0.4	−0.12	0.05	−5.28	−6.31	−1.32	−14.08	−0.07
0.7	−0.19	0.07	−8.88	−10.54	−7.63	−22.34	−0.1
0.9	−0.24	0.09	−11.14	−13.16	36.21	−33.6	−0.15
1.1	−0.27	0.1	−13.28	−15.62	−21.01	1.89	−0.17
1.4	−0.32	0.12	−16.31	−19.07	−40.46	−3.0	−0.21
1.6	−0.34	0.13	−18.22	−21.22	−26.08	−17.16	−0.2

B. Simulation Results

Having in mind the case where ϵ_2 is 2.1, it corresponds to the situation where the relative electric permittivity in group 1 is equal to the one in group 2. This scenario represents uniform thermal age and temperature all over the XLPE's domain, which probably coincides with an unaged cable at rest. So, the simulations' outputs were processed as described in section III-B, and then, the deviation from the case where $\epsilon_2 = 2.1$ calculated. These divergences are summarized in table IV.

Table IV shows that the XLPE's increase of the electric permittivity in the regions nearest to phase conductors causes changes in the pattern defined before. Although x_0 and y_0 variables do not seem to have a relation with the electric permittivity, beta increases, and alpha, a, b and θ decrease with the raise of this property. These variations are in the order of $+20\,\%$ for a and b and $+0.25\,\%$ for α, β and θ when permittivity increase from 2.1 to 3.7.

V. Water Trees

Since WTs are a very typical phenomenon in power cables and are considered a pre-breakdown process in the presence of moisture [6], Finite Element Method (FEM) simulations have been run to analyze if its formation can be detected.

WTs can be divided into two groups: the Vented WTs and the Bow-Tie WTs. However, since the Vented WTs are considered more threatening [6], all simulations are focused on

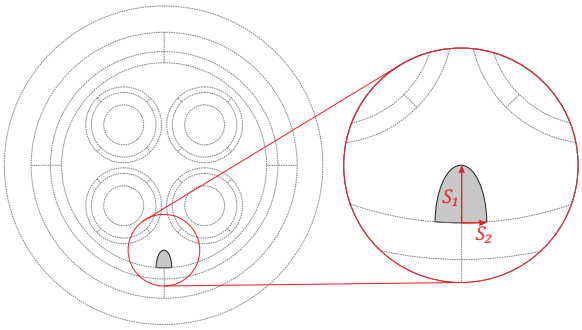

Fig. 9. Water tree sketch

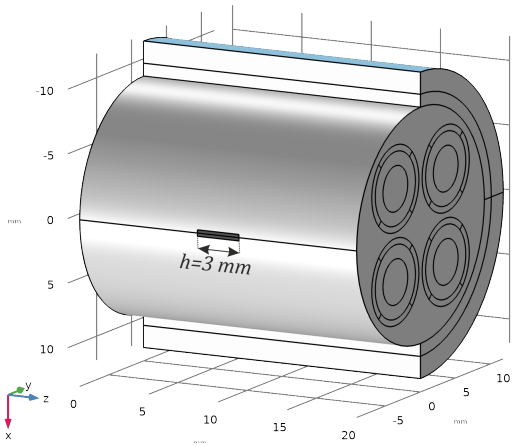

Fig. 10. 3D Model after water tree addition with $h = 3\,\mathrm{mm}$

this type. This option allows restricting the location of WT's root to the unbundling surfaces of the insulator.

A. Model Adjustments

After the definition of the global model of the power cable, the WT was introduced. For this, a new sketch plane was created, and in it, it was drawn a semi-ellipse, as it is represented in fig. 9. To note that, in fig. 9, the dotted lines are not present in the WT sketch, they are just auxiliary to show the relative position of the WT in the cable. Another aspect to have in mind is the fact that the WT location in this sketch will be changed to simulate different damaged zones. This semi-ellipse is characterized by two variables, s_1 and s_2, which correspond to its semi-axis length, as shown in fig. 9.

The sketched semi-ellipse is then extruded with a length of h in a way to centre the WT over cable length, producing a model similar to the one in fig. 10.

B. Water Tree Location

As referred before, the WTs analyzed in this study, the Vented-Water Trees, have their roots located in unbundling surfaces. So, multiple semi-ellipses' locations, representing damaged regions due to Vented WT were defined. fig. 11 shows these locations, which can be identified through an angle as it is in this figure.

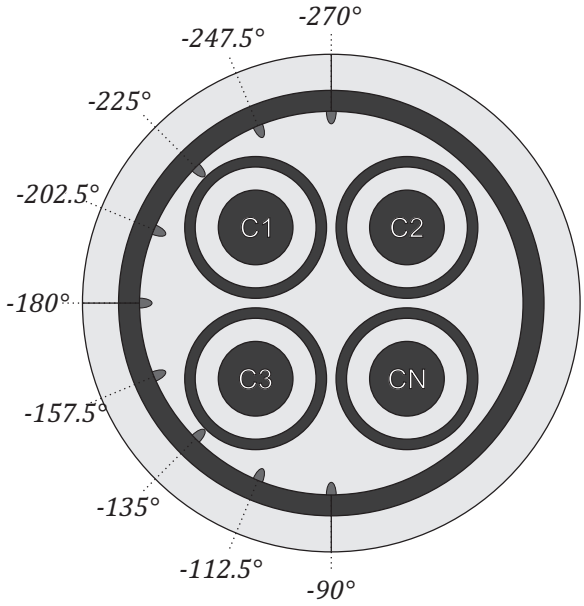

Fig. 11. Water trees locations

C. Water Tree 2D Simulation

Before using the 3D model, two 2D simulations of the cross-section presented in fig. 11 were developed, for each of the WT's locations. The difference between these two simulations is that in one of them, the relative electric permittivity applied to the WT's domain is 3.0 and in the other is 3.7, corresponding to different stages of the WT. In all the cases, the representation of the WT is a semi-ellipse with the semi-axis length of $s_1 = 0.6\,\mathrm{mm}$ and $s_2 = 0.25\,\mathrm{mm}$. The purpose of these tests is to check for variations that can identify the presence and the location of WT.

So, the seven parameters specified in section III, the output results of these simulations, were analyzed, and its relative deviation from a reference 2D case calculated. In fig. 12, it is plotted these variations in function of the WT's location.

When analyzing the graphs from fig. 12, it's visible that there are only relevant variations for the locations that are nearest to phase conductors, this is, at $-135°$ and $-225°$. Another point to note is the fact that the simulations in these locations affect different parameters, meaning that it is possible to distinguish which one is it. On the other hand, for the remaining locations, there are no evident variations, meaning that it is not possible to retrieve conclusions and therefore, suggesting that these WTs are not detectable.

D. Water Tree Size Simulation

To study the influence of the WT's size, various simulations where only the WT's dimension was changed were made. When it comes to the WT's location, three locations were chosen: the nearest zone to phase 3 conductor, at $-135°$, the region between Phase 3 and Neutral, at $-90°$, and the region between Phase 3 and Phase 1, at $-180°$. For all the cases, the

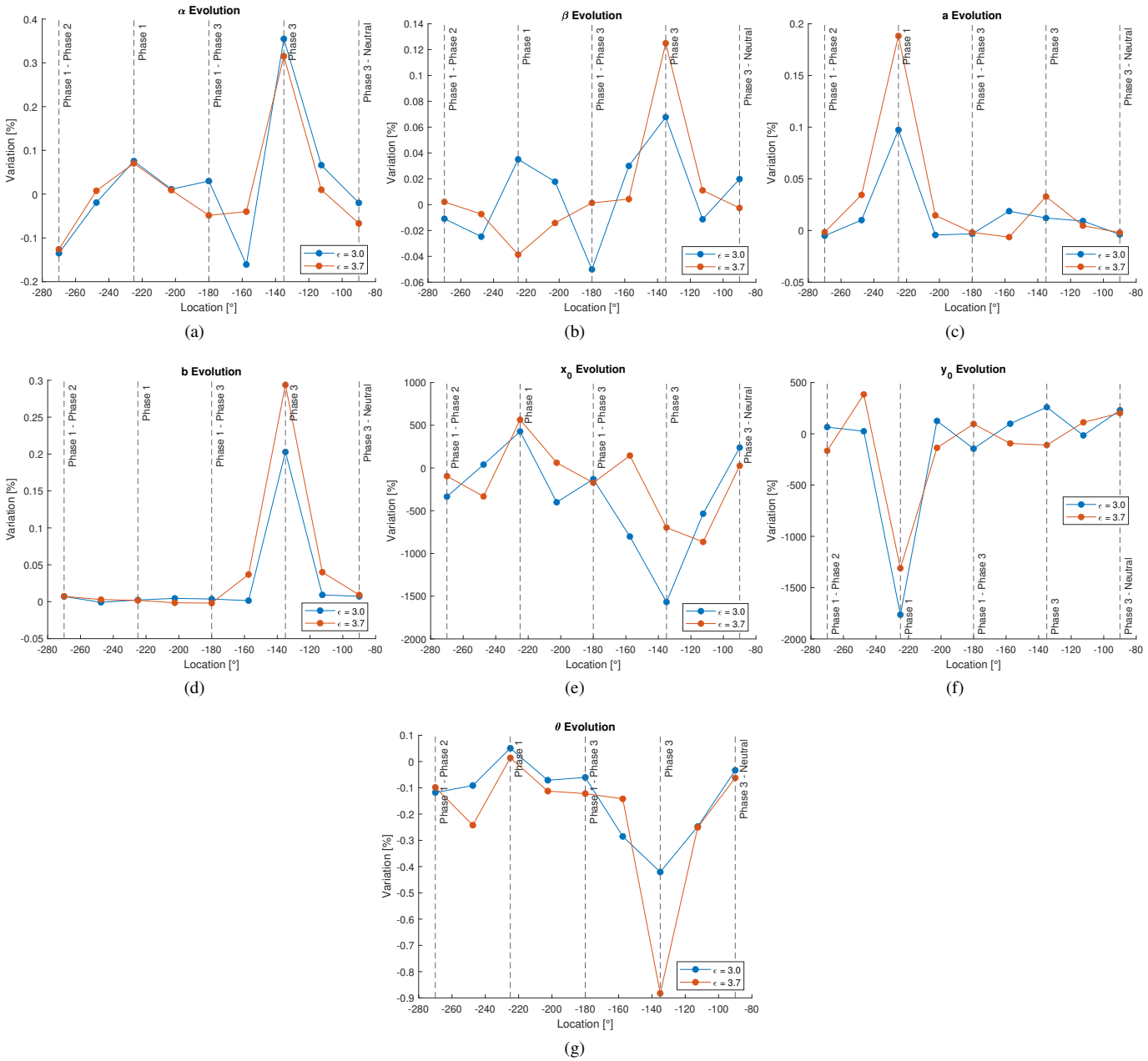

Fig. 12. Ellipse parameters evolution along with water tree location in 2D simulation: (a) α; (b) β; (c) a; (d) b; (e) x_0; (f) y_0; (g) θ

relative electric permittivity assigned to the WT's domain was 3.7.

Considering the WT's representation in this model is a prism, it's volume can be changed through the base area or prism's height. So, to study also which prism's characteristics have more influence in the results, simulations have been run with different dimensions of base area and prism's height. However, to be possible to simulate the same sizes in all the locations, the base area was changed by tuning only one of the ellipse's semi-axis, (s_2), while the other semi-axis (s_1) was fixed to $0.6\,\mathrm{mm}$. So, simulations have been run with the following sizes:

1) $V = 0.7\,\mathrm{mm}^3$ ($A = 0.23\,\mathrm{mm}^2$, $s_2 = 0.25\,\mathrm{mm}$, $h = 3\,\mathrm{mm}$);
2) $V = 2.1\,\mathrm{mm}^3$ ($A = 0.69\,\mathrm{mm}^2$, $s_2 = 0.75\,\mathrm{mm}$, $h = 3\,\mathrm{mm}$);
3) $V = 2.1\,\mathrm{mm}^3$ ($A = 0.23\,\mathrm{mm}^2$, $s_2 = 0.25\,\mathrm{mm}$, $h = 9\,\mathrm{mm}$);
4) $V = 4.1\,\mathrm{mm}^3$ ($A = 0.69\,\mathrm{mm}^2$, $s_2 = 0.75\,\mathrm{mm}$, $h = 6\,\mathrm{mm}$);
5) $V = 11.6\,\mathrm{mm}^3$ ($A = 1.28\,\mathrm{mm}^2$, $s_2 = 1.50\,\mathrm{mm}$, $h = 9\,\mathrm{mm}$);

These simulations outputs are displayed in fig. 13 to 15 for $-135°$, $-180°$ and $-90°$ locations, respectively. The bar graphs values, presented in these figures, represent the relative deviation from the reference values in table III.

1) Close to Phase Conductor 3 ($-135°$): In fig. 13 is a bar graph where it's possible to visualize the difference between simulation results. In this figure, each colour represents one of

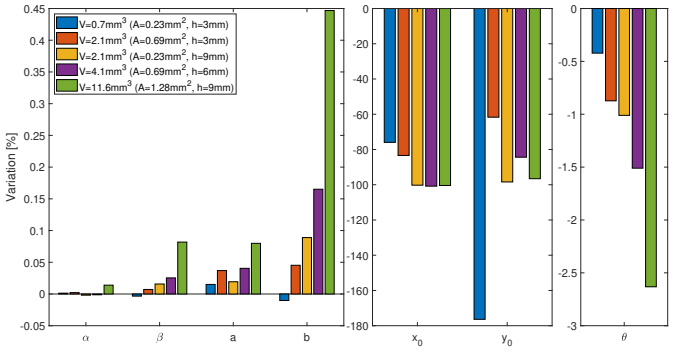

Fig. 13. Water tree size study results at $-135°$

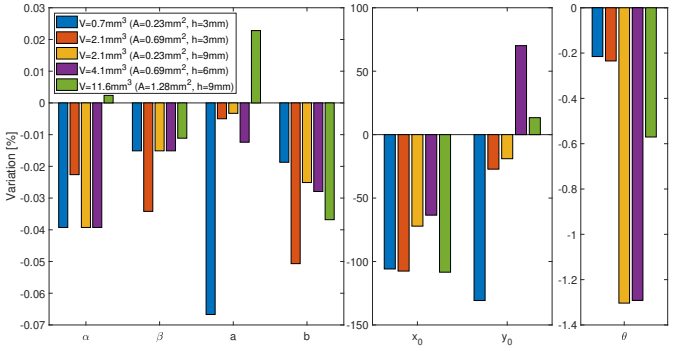

Fig. 14. Water tree size study results at $-180°$

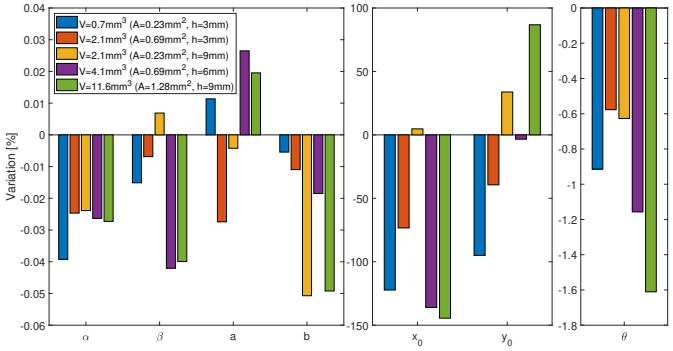

Fig. 15. Water tree size study results at $-90°$

the five cases, and each bar represents one parameter, allowing to have a better perspective on how the parameters change with the WT's size and which parameters are more affected. Since there are different ranges of variation, the seven parameters were distributed into three sub-graphs, to maintain visible the differences in the parameters with lower variations.

From these results, it's notable that the higher the WT's volume is, the higher will be the parameters variation of α, β, a, b and θ. Also, by comparing cases 2 and 3, it's possible to conclude that a WT height (h) increase has more influence when compared to an equal increment in the base area.

Finally, but not less important, is the fact that the trend of the various parameters' deviation with the WT's size matches the results from the two-dimensional model, presented in

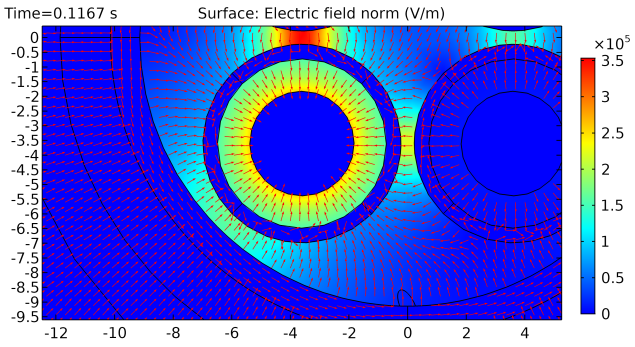

Fig. 16. Electric field direction

section V-C. The parameters that have a higher deviation in these results are the same that have more reliable peaks in figure 12 at $-135°$ location, meaning that the graphs from this figure are trustworthy.

2) Between Phase Conductor 3 and Phase Conductor 1 ($-180°$): The results from the simulations made with a WT located at $-180°$ are expressed in fig. 14. By inspecting it, it's visible that the amplitudes of deviations are much lower for this case. Also, there's not an apparent trend of evolution with the WT's volume increase, indicating the impossibility to detect a damaged region in this zone, like the 2D model simulations.

3) Between Phase Conductor 3 and Neutral ($-90°$): For this case, the WT is equidistant to conductor 3 and neutral, at $-90°$, and simulations results are presented in fig. 15. Like the previous case, there's no apparent trend for any parameter with the increase of the WT. Also, the range of these values is similar between these two cases. This range is so small that approximation errors start to be dominant, creating a dubious zone of results where no conclusions can be made, just like the WT simulations in the 2D model at this location.

E. Water Tree Growth Direction

The WTs' sizes from the previous section simulations were identical to all locations. So, since the available space at $-135°$ had more restrictions, the semi-axis s_1 was fixed to $0.6\,\mathrm{mm}$ for all the cases. However, for the locations where any conclusion could be reached, this restriction can be removed. On the other hand, WTs grow in the direction of the electric field [6], so since it points towards a conductor, as fig. 16 shows, the WTs in these locations will evolve towards one of the conductors.

Assuming γ as the angle between the direction of propagation of the water tree and the radial line which intersects the WT's root as shown in figure 17 scheme, γ was set to an amplitude of $30°$ and to point in the direction of phase 3 conductors.

Then, simulations were made for the locations of $-90°$ and $-180°$ with the same WT representation but with different sizes. In this case, to verify also the possibility of these WTs become detectable as they get closer to phase conductors, the WTs' dimensions in these simulations were the following:

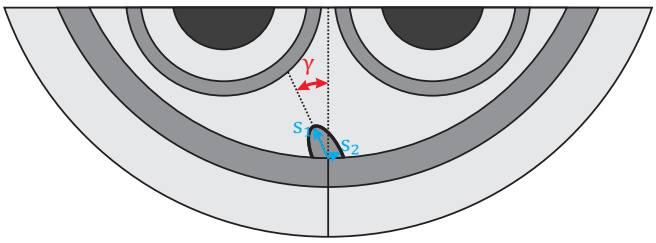

Fig. 17. Water tree growth direction scheme

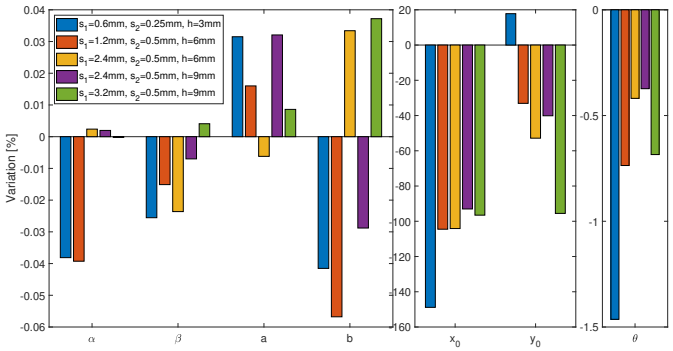

Fig. 18. Rotated water tree at $-90°$ bar graph results

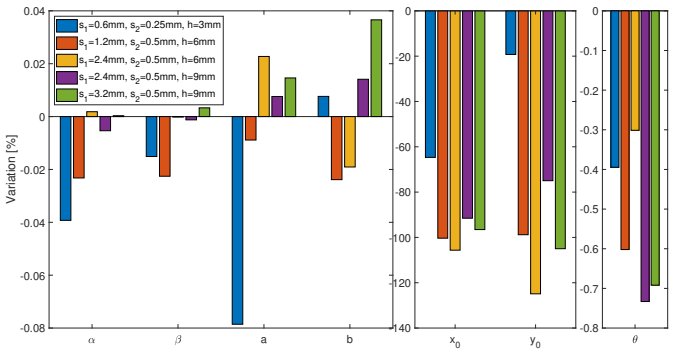

Fig. 19. Rotated water tree at $-180°$ bar graph results

1) $s_1 = 0.6\,\text{mm};\ s_2 = 0.25\,\text{mm};\ h = 3\,\text{mm};$
2) $s_1 = 1.2\,\text{mm};\ s_2 = 0.50\,\text{mm};\ h = 6\,\text{mm};$
3) $s_1 = 2.4\,\text{mm};\ s_2 = 0.50\,\text{mm};\ h = 6\,\text{mm};$
4) $s_1 = 2.4\,\text{mm};\ s_2 = 0.50\,\text{mm};\ h = 9\,\text{mm};$
5) $s_1 = 3.2\,\text{mm};\ s_2 = 0.50\,\text{mm};\ h = 9\,\text{mm};$

The output results of these simulations are presented in fig. 18 and 19, for the $-90°$ and $-180°$ locations, respectively.

When inspecting these two figures, it is visible that for both locations, the variation ranges are pretty small, like the simulations in the previous section. Also, there's no visible trend which may indicate a relation between the output variables and the WT's dimension, meaning that the WTs in these locations are not detectable.

VI. Analysis of the Results

In the previous sections, simulations of power cables in predetermined conditions were made to check how some variables would change. Based on this, it is intended to do the reverse process, estimate the power cable's status through the analysis of those variables changes.

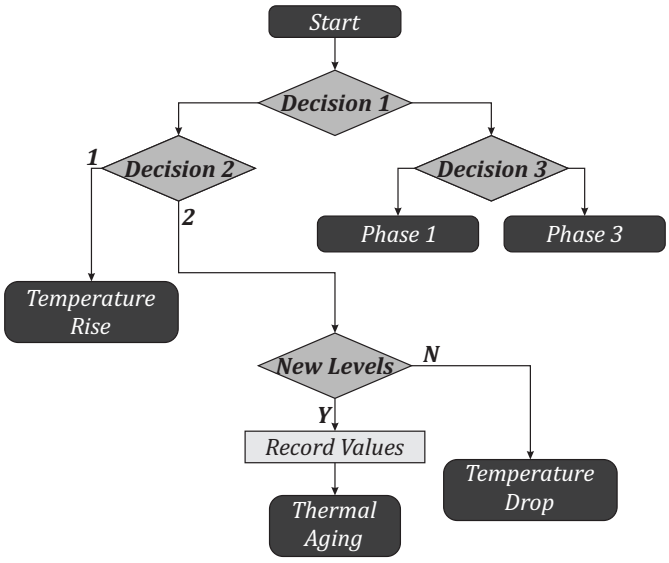

Fig. 20. Proposed methodology flowchart

TABLE V
Decision 1 BLOCK CONDITIONS

Thermal Aging	**Water Tree**	
$\lvert\Delta a\rvert > 1\%$	$\Delta a > 0.1\%$	$\lvert\Delta a\rvert < 0.1\%$
$\lvert\Delta b\rvert > 1\%$	$\lvert\Delta b\rvert < 0.1\%$	$\Delta b > 0.1\%$
$\Delta a \times \Delta b > 0$	-	-

In this section, a methodology for this goal is proposed. This methodology is summarized in fig. 20 flowchart and has three decision blocks that will be discussed.

A. Decision 1 Block - Thermal Aging vs Water Tree

Since the simulations made can be divided into two groups of deterioration, thermal ageing and/or *water trees* occurrence, the first step will be to establish a process that allows distinguishing these two groups.

From section IV and V, it was verified that the parameters more trustworthy were a and b, considering the higher deviation and the less noise in the WT simulations case. For these parameters, it was noted that for thermal ageing both a and b change in the same direction, while for the WT case, only one of these parameters changes. It was also detected that the variation of these parameters is more intense for the thermal ageing than for the WT simulations. So, the conditions from *Decision 1* block from fig. 20 can be summarized as in table V.

B. Decision 2 Block - Thermal Ageing

As verified in section II-A, this pattern of variation could be provoked by thermal ageing or by temperature variation. So, it is necessary to estimate the real cause of this type of parameters variation.

In case there's an increase of α, a, b and θ and a decrease of β, there's no doubt that it reflects a temperature rise. However, the opposite case, where α, a, b and θ decrease and β increase,

TABLE VI
Decision 2 BLOCK CONDITIONS

Output 1	Output 2
$\Delta\alpha > 0$	$\Delta\alpha < 0$
$\Delta\beta < 0$	$\Delta\beta > 0$
$\Delta a > 0$	$\Delta a < 0$
$\Delta b > 0$	$\Delta b < 0$
$\Delta\theta > 0$	$\Delta\theta < 0$

TABLE VII
Decision 3 BLOCK CONDITIONS

Phase 1	Phase 3
$\Delta a > 0$	$\Delta b > 0$
$\Delta y_0 < 0$	$\Delta\alpha > 0$
-	$\Delta\beta > 0$
-	$\Delta\theta < 0$

can indicate a temperature drop or thermal ageing. Having in mind that ageing is an irreversible process and a temperature change not, this means that although these parameters may oscillate between a range of values due to temperature changes, this range may change due to ageing, meaning that parameters will reach new values. So, a simple methodology could be recording parameters values over time. This way, when these parameters' values reached unprecedented levels, this would indicate ageing of the cable. This process corresponds to the section from *Decision 2* block to down, from the flowchart of fig. 20, and the conditions for *Decision 2* block are expressed in table VI.

C. Decision 3 Block - Water tree

After detecting the existence of a WT, it can be possible to estimate the location of the WT in the cable, using the same data. From the obtained results, only the WTs near conductors were detected, but, they affected the results in different ways. When near from phase 1 conductors, the parameter a has increased and the y_0 declined. When near from phase 3 conductors, parameters b, α and β has increased while θ has decreased. This pattern can be used to distinguish the nearest conductor from the affected zone through a simple check, represented as *Decision 3* in fig. 20 flowchart, and summarized in table VII.

VII. Conclusion

A. Achievements

This work aimed to develop an alternative methodology capable of predicting a power cable fault through a system that could be installed, without interfering, under already operating networks and based in electric variables. Some phenomenons, responsible for the degradation of this component, were studied and the simulated.

For the case of thermal ageing, the FEMS simulations allowed to detect a pattern, that could be used to identify this phenomenon based on electric variables. However, temperature variations can also cause the same pattern, so, the addition of temperature data would allow more accuracy to the proposed methodology.

This work also developed simulations for the case of the WT phenomenon, using 2D and 3D models. These simulations allowed to identify a new pattern when the WT were located in the nearest regions from phase conductors. For all the cases the variations were relatively small, but for the simulations with the smallest WTs' sizes, the output results start to be more affected by noise from the computational errors and approximations, forbidding any possible conclusion. It means that only from certain sizes the WT become detectable.

When it comes to the remaining WT's locations, additional simulations were developed to investigate a criterion that could identify them, however without success.

B. Future Work

Based on the exhibited work, and since it still needs developments, this section has some guidelines for future steps:

- Simulate harmonics in the applied voltages and analyze how it affects the results;
- Introduction of an acquiring system for temperature data to better distinguish the thermal ageing from the temperature variations and to have more information from operation conditions;
- Analyze how is the soil's moisture in the surrounding region of a power cable and how it can vary with weather phenomena and then highlight WTs.

To note that these guidelines are just suggestions and are targeted to the phenomenons studied in this work. Other occurrences and other purposes can be studied and would contribute to the value of the proposed.

References

[1] G. Ye, C. Cai, B. Zhou, and M. Ye, "Simulation of electrical trees in XLPE cable insulation and electric field analysis," *The Journal of Engineering*, vol. 2019, no. 16, pp. 1882–1885, 2019, ISSN: 2051-3305. DOI: 10.1049/joe.2018.8704.

[2] S. Konglysan and W. Rungseevijitprapa, "XLPE Insulated High Voltage Underground Cable Assessment of Leakage Current Studies," *International Journal of Computing, Communication and Instrumentation Engineering*, vol. 2, no. 2, pp. 162–164, 2015. DOI: 10.15242/ijccie.er1015112.

[3] Y. Mecheri, L. Boukezzi, A. Boubakeur, and M. Lallouani, "Dielectric and mechanical behavior of Cross-Linked Polyethylene under thermal aging," *Conference on Electrical Insulation and Dielectric Phenomena (CEIDP), Annual Report*, vol. 2, pp. 560–563, 2000, ISSN: 00849162. DOI: 10.1109/CEIDP.2000.884022.

[4] I. Radu, M. Acedo, J. C. Filippini, P. Notingher, and F. Frutos, "The effect of water treeing on the electric field distribution of XLPE: Consequences for the dielectric strength," *IEEE Transactions on Dielectrics and Electrical Insulation*, vol. 7, no. 6, pp. 860–868, 2000, ISSN: 10709878. DOI: 10.1109/94.892001.

[5] Y. J. Han, H. M. Lee, and Y. J. Shin, "Thermal aging estimation with load cycle and thermal transients for XLPE-insulated underground cable," *Annual Report - Conference on Electrical Insulation and Dielectric Phenomena, CEIDP*, vol. 2017-Octob, pp. 205–208, 2018, ISSN: 00849162. DOI: 10.1109/CEIDP.2017.8257566.

[6] T. Boonraksa, N. Promvichai, T. Supanarapan, K. M. Minja, P. V. Chombo, and B. Marungsri, "Simulation of Electric Field Distribution in Water Treed XLPE HV Underground Cable Using COMSOL Multiphysics," in *Proceedings of the IIAE International Conference*, 2017, pp. 267–270. DOI: 10.12792/iciae2017.048.